AGU PUBLICATIONS

Water Resources Research

RESEARCH ARTICLE
10.1002/2013WR014639

Key Points:
- Satellite soil moisture holds potential for calibration of hydrological models
- Soil moisture observations enable better calibration of land-surface parameters
- Errors in discharge simulations are reduced using soil moisture for calibration

Correspondence to:
N. Wanders,
n.wanders@uu.nl

Citation:
Wanders, N., M. F. P. Bierkens, S. M. Jong, A. Roo, and D. Karssenberg (2014), The benefits of using remotely sensed soil moisture in parameter identification of large-scale hydrological models, *Water Resour. Res.*, *50*, 6874–6891, doi:10.1002/2013WR014639.

Received 23 AUG 2013
Accepted 1 AUG 2014
Accepted article online 7 AUG 2014
Published online 22 AUG 2014
Corrected 15 SEP 2014

This article was corrected on 15 SEP 2014. See the end of the full text for details.

The benefits of using remotely sensed soil moisture in parameter identification of large-scale hydrological models

N. Wanders[1], M. F. P. Bierkens[1,2], S. M. de Jong[1], A. de Roo[1,3], and D. Karssenberg[1]

[1]Department of Physical Geography, Utrecht University, Utrecht, Netherlands, [2]Deltares, Utrecht, Netherlands, [3]European Commission, Joint Research Centre, Institute for Environment and Sustainability, Ispra, Italy

Abstract Large-scale hydrological models are nowadays mostly calibrated using observed discharge. As a result, a large part of the hydrological system, in particular the unsaturated zone, remains uncalibrated. Soil moisture observations from satellites have the potential to fill this gap. Here we evaluate the added value of remotely sensed soil moisture in calibration of large-scale hydrological models by addressing two research questions: (1) Which parameters of hydrological models can be identified by calibration with remotely sensed soil moisture? (2) Does calibration with remotely sensed soil moisture lead to an improved calibration of hydrological models compared to calibration based only on discharge observations, such that this leads to improved simulations of soil moisture content and discharge? A dual state and parameter Ensemble Kalman Filter is used to calibrate the hydrological model LISFLOOD for the Upper Danube. Calibration is done using discharge and remotely sensed soil moisture acquired by AMSR-E, SMOS, and ASCAT. Calibration with discharge data improves the estimation of groundwater and routing parameters. Calibration with only remotely sensed soil moisture results in an accurate identification of parameters related to land-surface processes. For the Upper Danube upstream area up to 40,000 km^2, calibration on both discharge and soil moisture results in a reduction by 10–30% in the RMSE for discharge simulations, compared to calibration on discharge alone. The conclusion is that remotely sensed soil moisture holds potential for calibration of hydrological models, leading to a better simulation of soil moisture content throughout the catchment and a better simulation of discharge in upstream areas.

1. Introduction

Soil moisture plays a crucial role in the hydrological cycle, modulating evapotranspiration, overland flow, and groundwater replenishment. As a consequence, an accurate simulation of discharge with hydrological models requires good quality estimates of soil moisture content. Especially in situations with a precipitation amount close to the storage capacity of the unsaturated zone, the soil moisture content has a large impact on whether overland flow will occur and the amount of overland flow generated [*Merz and Plate*, 1997; *Penna et al*., 2011]. However, soil moisture content is highly variable in time and space [*Western et al*., 2002] and ground-observations are still limited [*Dorigo et al*., 2011].

Remotely sensed soil moisture provides observations with a high temporal resolution and a large spatial extent. Satellite soil moisture observations are therefore increasingly used for calibration of hydrological models and the identification of parameters related to land-surface processes [e.g., *Santanello et al*., 2007; *Montzka et al*., 2011; *Sutanudjaja et al*., 2013]. Moreover, in areas with a low coverage of precipitation measurements, remotely sensed soil moisture can give valuable information on the spatial distribution and the intensity of precipitation events [*Crow et al*., 2009]. Thus, when used in real time, remotely sensed soil moisture observations have the potential to increase flood forecasting accuracy [*Komma et al*., 2008; *Hendricks Franssen et al*., 2011].

Due to the large data volumes, coarse spatial resolution and its complicated error structure, the use of near real-time remotely sensed soil moisture has not yet been fully explored by hydrologists. In numerical weather forecasting and unsaturated zone modeling, the assimilation of remotely sensed soil moisture for hydrological and atmospheric simulations has showed promising results [e.g., *Pauwels et al*., 2001; *Reichle et al*., 2002; *Scipal et al*., 2008; *Bolten et al*., 2010; *Brocca et al*., 2010; *Liu et al*., 2011; *Dharssi et al*., 2011; *Draper et al*., 2011; *Brocca et al*., 2012; *Draper et al*., 2012; *de Rosnay et al*., 2013]. For large-scale catchments, *Draper et al*. [2011] assimilated remotely sensed soil moisture from the Advanced Scatterometer (ASCAT) over France to improve

discharge simulations. It was concluded that the assimilation of soil moisture mainly corrected for biases in precipitation or incorrect model climatology. Several studies used in situ observations of soil moisture or synthetic simulations of remotely sensed soil moisture to show that using these observations in model calibration could significantly change the parameter values of the model [e.g., *Aubert et al*., 2003; *Santanello et al*., 2007; *Lü et al*., 2011; *Montzka et al*., 2011]. These studies were performed in catchments smaller or slightly larger than the typical resolution of microwave satellites (626–2500 km^2), and therefore do not allow to evaluate the added value of remotely sensed soil moisture for model calibration over a range of spatial scales and especially scales larger than the spatial resolution of the sensors. A recent study over a larger spatial domain by *Sutanudjaja et al*. [2014] used a brute force calibration of a large-scale hydrological model for the Rhine and Meuse river basin using data from the ERS scatterometer. It was shown that, using remotely sensed soil moisture, the parameters related to the percolation through the unsaturated zone could be improved to yield a better simulation of the soil moisture content. However, discharge simulations were not improved.

The aim of this study is to investigate the benefits of multisensor remotely sensed soil moisture observations in parameter identification in large-scale hydrological models using detailed error estimates on satellite soil moisture observations. To achieve this aim, this research focuses on two main research questions: (i) Which parameters of hydrological models can be identified by calibration with remotely sensed soil moisture? (ii) Does calibration with remotely sensed soil moisture lead to an improved calibration of hydrological models compared to approaches that calibrate only with discharge, such that this leads to improved simulations of soil moisture content and discharge? To address these questions, the LISFLOOD [*Van Der Knijff et al*., 2010] large-scale hydrological model is used to simulate discharge and soil moisture for the Upper Danube catchment, which contains parts of Austria, Germany, and the Czech Republic. LISFLOOD is the underlying model used in the European Flood Awareness System (EFAS) and is used in operational flood forecasting in Europe [*Thielen et al*., 2009; *Bartholmes et al*., 2009]. The model is calibrated in this study using remotely sensed soil moisture observations from the Advanced Microwave Scanning Radiometer-EOS (AMSR-E), Soil Moisture and Ocean Salinity (SMOS), and ASCAT and discharge observations for the period 2010–2011. Also combinations of calibration on discharge and all satellites sensors are performed, to study the added value of the remotely sensed soil moisture when discharge observations are readily available. Error structures for the different sensors and their error cross covariance are retrieved from a previous study of *Wanders et al*. [2012]. The impact of the new calibration on the soil moisture simulations is studied and a validation on multiple discharge locations is performed. Compared to previous work, our study contains the following new elements: (i) It is the first time that real remotely sensed data are used for calibration of a large-scale distributed hydrological model. (ii) The use of multiple sensors is new, which allows to compare the relative benefit of the different products, also compared to using discharge only. (iii) Using a probabilistic data assimilation framework for calibration and state estimation is new, in particular taking into account the full retrieval error structure and cross covariance between multiple sensors. The latter enables optimal weighting between their different information sources, potentially leading to improved calibration.

2. Material and Methods

2.1. Study Area

In this study, the Upper Danube catchment up to Bratislava (catchment size $135\times10^3 km^2$, Figure 1) is used for the calibration (state updating and parameter identification) of the LISFLOOD model. The border of the Upper Danube consists of the Alps in the south and the catchment contains the northern part of Austria, the southern part of Germany, the south-eastern part of the Czech Republic, and western Slovakia. Elevations range from 150 to 3150 mean annual sea level. The soil mostly consists of loamy sediments and approximately 35% of the area is covered with forest. In the catchment, daily discharge observations for 23 locations are available through the Global Runoff Data Centre (GRDC) over 2000–2011.

Meteorological input was obtained from high density interpolated ground data from various national meteorological services made available by the Joint Research Centre [*Ntegeka et al*., 2013]. The data were interpolated with an Inverse Distance Weighting [IDW, *Shepard*, 1968] approach instead of kriging, since this could generate errors if not well controlled in a real-time spatial interpolation. Time series of approximately 200 meteorological stations were used to create the spatially interpolated meteorological variables. The total precipitation over the period 2001–2011 in the catchment is approximately 920 mm y^{-1} and total actual

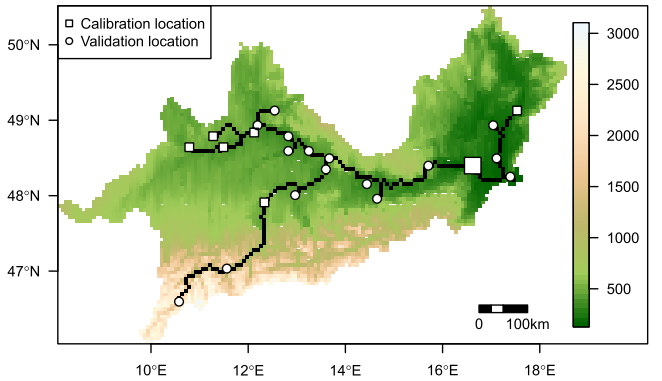

Figure 1. Digital elevation map of the Upper Danube catchment, colors indicate elevation (m), indicated in black is the river network, square symbols indicate locations for calibration on discharge observations, and circles indicate locations for validation on discharge observations. The large square near the outlet (right) is the location used for calibration if only one discharge time series is used.

evapotranspiration is approximately 630 mm y^{-1}. The runoff ratio of the catchment is 0.31, where a total of approximately 290 mm y^{-1} leaves the catchment as discharge at Bratislava, of which approximately 22 mm y^{-1} on average is generated as surface runoff. Moreover, in the mountainous areas, this amount of surface runoff is in general much higher than in the lower areas near the main stream of the Danube.

2.2. Hydrological Model

The hydrological model LISFLOOD [*Van Der Knijff et al.*, 2010] was used for the calibration and validation of soil moisture and discharge simulations. LISFLOOD is a hydrological rainfall-runoff-routing model running in the PCRaster modeling environment [*Wesseling et al.*, 1996; *Karssenberg et al.*, 2010]. LISFLOOD is used in the operational EFAS of the European Commission for medium range flood forecasting of large river basins in Europe [*Thielen et al.*, 2009; *Bartholmes et al.*, 2009]. The meteorological forcing of LISFLOOD consists of daily precipitation, daily potential evapotranspiration, and the average daily temperature. The model originally consists of a vegetation layer, two layers for the unsaturated zone, one fast responding and one slow responding linear groundwater reservoir and a channel network for discharge routing (Figure 2). The kinematic wave equation is used for discharge routing using an hourly time step for both surface runoff to the channel network and routing within the channel network.

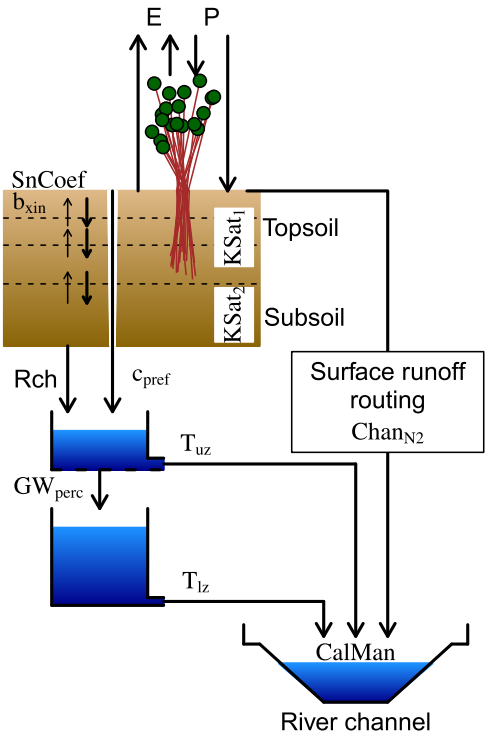

Figure 2. LISFLOOD model setup, precipitation (*P*), evaporation (*E*), snowmelt coefficient (*SnCoef*), Xinanjiang shape parameter (b_{xin}), saturated conductivity of the topsoil ($KSat_1$), saturated conductivity of the subsoil ($KSat_2$), empirical shape parameter preferential macropores flow (c_{pref}), recharge from the unsaturated zone to the groundwater (*Rch*), maximum percolation rate from upper to lower groundwater (GW_{prec}), reservoir constant upper groundwater (T_{uz}), reservoir constant lower groundwater (T_{lz}), surface runoff roughness coefficient ($Chan_{N2}$), and Channel Manning's roughness coefficient (*CalMan*).

For this study, a number of modifications have been made to the LISFLOOD model. To enable a more detailed modeling approach of the soil moisture in the topsoil, two additional unsaturated zone layers have been added to the original LISFLOOD model, which also enables direct comparison and assimilation of each of the satellite products. The upper two layers are 2 and 3 cm thick, respectively, and the third layer represents the remaining part of the rooting depth (first three layers together are hence referred to as the topsoil, Figure 2). The root zone is simulated using the first three layers of the unsaturated zone and evapotranspiration occurs from these layers. The evaporation for a particular layer is limited if soil moisture is below critical soil moisture conditions, in which case more water is extracted from the other soil moisture layers to compensate for the reduced evaporation. Critical soil moisture conditions are calculated from the local soil properties [*Panagos*., 2012]. The abstraction per layer is linearly related to the total storage capacity of the layer. Thick layers will thus have a larger contribution

Table 1. Calibration Parameters and the Range of Their Prior Normal Distributions, the Bottom Half Is Only Calibrated Using Discharge Observations[a]

Parameter	Description	Unit	Prior
SnCoef	Snowmelt rate	mm d^{-1}	0.1–10
$KSat_1$	Multiplier of unsaturated conductivity topsoil		0.9–15
$KSat_2$	Multiplier of unsaturated conductivity subsoil		0.9–22
c_{pref}	Empirical shape parameter preferential macropore flow	mm	0.1–2.3
b_{xin}	Xinanjiang shape parameter related to saturation degree		0.05–0.7
T_{uz}	Linear reservoir constant upper groundwater	Days	1.5–40
T_{lz}	Linear reservoir constant lower groundwater	Days	500–2500
GW_{perc}	Maximum percolation rate, upper to lower groundwater	mm d^{-1}	0.3–1.8
$Chan_{N2}$	Multiplier on surface roughness for surface runoff		0.1–7.2
CalMan	Multiplier on channel Manning's roughness coefficient		0.1–2.0

[a] T_{uz} and T_{lz} are divided into three different zones namely, steep, intermediate, and flat areas. More details can be found in section 2.2.

to the evapotranspiration compared to thinner layers. When the entire root zone is below critical soil moisture conditions, the evaporation is limited for the entire topsoil and actual evapotranspiration will be lower than potential evapotranspiration. Bare soil evapotranspiration will occur only from the first layer of 2 cm. Via capillary rise replenishment of the root zone can occur from the subsoil. The amount of capillary rise depends on the difference in hydraulic head of two layers and the average conductivity of the layers. Subdaily time steps are included to enable a stable performance of the soil moisture simulation, where the number of subdaily time steps is dependent on the amount of infiltration and water storage in the unsaturated zone. For a more detailed description of the original LISFLOOD model and a full description of the equations, the reader is referred to *Van Der Knijff et al*. [2010].

The parameters calibrated are given in Table 1, combined with the range of the prior normal distribution before calibration. The same set of parameters is used to calibrate EFAS and a sensitivity analysis for each of these parameters has been performed for every new version of the LISFLOOD model [*Van Der Knijff et al*., 2010]. Thus, the same set of parameters was subject to calibration in this study. The mean of the prior normal distribution for the model parameters is determined by the original LISFLOOD calibrated parameters. Since the distribution of parameter errors is unknown, a normal distribution with a standard deviation of 20% of the mean parameter value is used to generate ensemble member realizations for the Ensemble Kalman Filter. Realizations outside the possible parameter range (e.g., negative saturated hydraulic conductivity) are rejected and replaced by new realizations. The prior distribution is used to determine the baseline scenario to which the other scenarios are compared and evaluated. For the reservoir constant of upper and lower groundwater (T_{uz}, T_{lz}), three spatially distributed values are identified in the calibration because groundwater response throughout the catchment may be significantly different. Therefore, the catchment is divided into three groundwater regions: locations with a terrain gradient of $\geq$ 15% are classified as steep, areas with a gradient between 5 and 15% are classified as intermediate, and areas with gradients $\leq$ 5% are classified as the flat areas. The division in groundwater regions is made since in the mountainous (steep) areas aquifers are shallow and groundwater response will be faster compared to the flat lowland areas.

2.3. Data

2.3.1. Satellite Data

Remotely sensed soil moisture data from three satellites are used, namely SMOS, ASCAT, and AMSR-E (Table 2). SMOS is the first dedicated soil moisture satellite using fully polarized passive microwave signals at 1.41 GHz (L-band) observed at multiple angles [*Kerr et al*., 2012]. The observation depth of SMOS is up to 5 cm with a spatial resolution of 35–50 km depending on the incident angle and the deviation from the satellite ground track. SMOS retrievals which are potentially contaminated with Radio Frequency Interference (RFI) have been removed.

AMSR-E is a multifrequency passive microwave radiometer (6.9 GHz, C-band) and is a widely used sensor for soil moisture retrievals. The spatial resolution of AMSR-E is between 36 and 54 km with an observation depth of 2 cm and a revisit time of 3 days. Several algorithms estimating surface soil moisture from AMSR-E observations exist [e.g., *Njoku et al*., 2003; *Owe et al*., 2008; *Pan et al*., 2014]. One of the algorithms using exclusively satellite observations is the Land Parameter Retrieval Model (LPRM), which was used for this

Table 2. General Sensor Properties Relevant for This Study[a]

	SMOS	ASCAT	AMSR-E
Frequency (GHz)	1.41	5.3	6.9
Microwave type	Passive	Active	Passive
Spatial resolution (km)	35–50	25	36–54
Max revisit time (days)	3	3	3
Observation depth (cm)	0–5	0–2	0–2
Descending overpass (h)	6:00 P.M.	9:30 A.M.	1:30 A.M.
Observation error ($m^3\ m^{-3}$)	0.057	0.051	0.049
Number of observations	92,000	223,000	81,000

[a]Satellite errors are derived from *Wanders et al.* [2012].

study. LPRM soil moisture products have been validated against in situ observations [e.g., *Wagner et al.*, 2007; *De Jeu et al.*, 2008; *Draper et al.*, 2009], models [e.g., *Loew et al.*, 2009; *Crow et al.*, 2010; *Bisselink et al.*, 2011; *Wanders et al.*, 2012], and other satellite products [e.g., *Wagner et al.*, 2007; *Dorigo et al.*, 2010].

Unlike SMOS and AMSR-E, ASCAT uses active microwave at a frequency of 5.3 GHz (C-band) to determine the soil moisture content [*Wagner et al.*, 1999; *Naeimi et al.*, 2009]. ASCAT uses a change detection method [*Naeimi et al.*, 2009] and data are provided relative to the soil moisture content of the wettest (field capacity) and driest (wilting point) soil moisture conditions measured [*Wagner et al.*, 1999]. The spatial resolution of ASCAT is around 25 km, the observation depth is 2 cm, and the temporal resolution equals a revisit time of 3 days.

All satellite soil moisture products are used on an equal area Discrete Global Grid product (DGG). For the SMOS and ASCAT soil moisture retrieval time series, a DGG is available. AMSR-E data were projected on the DGG of SMOS using the nearest neighbor approach, because both satellites have roughly the same spatial resolution. The DGG of ASCAT uses equally spaced areas of 12.5 km while the other DGG uses a slightly lower resolution of 15 km between points.

Although the passive microwave satellite missions, SMOS and AMSR-E, give absolute soil moisture values in $m^3\ m^{-3}$, all satellite data were converted to relative soil moisture. The relative soil moisture values are calculated compared to the model climatology, to remove systematic biases between observations and model simulations. The converted satellite values $\theta_{s,new}$ in $m^3\ m^{-3}$ used for calibration are calculated by

$$\theta_{s,new} = \frac{\theta_s - \theta_{s,5}}{\theta_{s,95} - \theta_{s,5}} (\theta_{FC} - \theta_{WP}) + \theta_{WP} \quad (1)$$

where θ_s are the observed satellite soil moisture values ($m^3\ m^{-3}$ or –), $\theta_{s,95}$ and $\theta_{s,5}$ are the 95th and 5th percentiles of satellite soil moisture values per DGG location, respectively ($m^3\ m^{-3}$ or –), and θ_{FC} and θ_{WP} are field capacity and wilting point of the modeled soil moisture values ($m^3\ m^{-3}$). The average model values, θ_{FC} and θ_{WP}, are calculated using the model average over the support unit of the satellite retrieval.

Frozen soils, snow accumulation, and Radio Frequency Interference (RFI) hamper the soil moisture retrieval due to changes in the dielectric constant when water freezes. Therefore, retrievals done with (1) an air temperature below 4°C, (2) simulated snow accumulation, and (3) the presence of RFI (mainly for SMOS) and (4) a retrieval uncertainty for SMOS (*DQX*) of $\geq$0.04 $m^3\ m^{-3}$ were not used in the calibration. Retrievals under one of the above conditions will be unreliable and would lead to incorrect calibration of the hydrological model. The temperature data were derived from the observed data and snow conditions were derived from the model simulation.

2.3.2. Discharge Data

The Upper Danube catchment contains 23 locations where daily discharge observations are available. Time series of discharge are available from January 2000 until December 2011. Using a split sample approach, the model parameters are calibrated using 7 stations and validated against 16 stations which are situated throughout the catchment of the Upper Danube (Figure 1). Calibration and validation stations are selected such that they are equally distributed over the catchment and are situated in both small streams and the main stream of the Upper Danube.

2.4. Data Assimilation

The Ensemble Kalman Filter (EnKF) is a Monte Carlo-based approach which is highly suitable for data assimilation and model calibration in high dimensional systems [*Evensen*, 1994; *Burgers et al.*, 1998; *Evensen*, 2003, 2009], like the LISFLOOD model. Due to the Monte Carlo approach, the model uncertainties in the EnKF can be calculated from the ensemble spread. In order to reduce calculation time, it is assumed that the ensemble

spread is significantly large to simulate the true uncertainty of the simulation. When the ensemble size is too low, the tails of the distribution are most likely not simulated correctly and ensemble uncertainty is underestimated. An advantage of the EnKF is that it does not require propagation of the error covariance matrix as the standard Kalman Filter would require. This eliminates the need for a complex forward error model which needs to be run parallel to the model simulations. Compared to the 4DVAR [*Le Dimet and Talagrand*, 1986] assimilation technique, the advantage is that there is no need for an adjoint state model to invert the model state into the period before assimilation. In contrast to the particle filter [*Van Leeuwen*, 2009], the EnKF can be used with a lower number of members, because the risk of particle collapse and ensemble deterioration is not as high as for the particle filter. These properties of the EnKF make it highly suitable for complex spatially distributed models, with long calculation times, a large number of calibration parameters and state variables. The EnKF has been successfully applied for flood forecasting with assimilation of discharge observations [e.g., *Weerts and El Serafy*, 2006; *Clark et al*., 2008; *Komma et al*., 2008; *Camporese et al*., 2009; *Pauwels and De Lannoy*, 2009; *Mendoza et al*., 2012; *Rakovec et al*., 2012; *McMillan et al*., 2013]. Additionally, the current EnKF setup can be used to do forecasts in an operational flood forecasting framework, without changing the model setup and preserving the model uncertainties [e.g., *Wanders et al*., 2014].

With a total of 300 ensemble members, the EnKF is applied to update state variables and identify parameters (Figure 3 and Table 1) of the hydrological model LISFLOOD (Figure 2). The perturbation of each parameter has been described in section 2.2, while the initial model states are determined based on a 10 year open loop simulation of LISFLOOD with the perturbed parameters. A 10 year period is used to ensure that the deep groundwater simulations would no longer be influenced by the initial conditions. The forward LISFLOOD model is given by

$$\Psi(t+1)=f(\Psi(t),F(t),p) \tag{2}$$

where $\Psi(t)$ is the state of the model at time t, $F(t)$ the model forcing at time t (e.g., precipitation and evaporation), and p are the model parameters. The EnKF is applied on each daily time step using observations from remote sensing (AMSR-E, SMOS, and ASCAT) and discharge observations. The general form of the EnKF is given by *Evensen* [2003]. It can be formalized by the model forecast (Ψ^f), given by

$$\Psi^f=(\psi_1^f,\ldots,\psi_{nens}^f) \tag{3}$$

where $\psi_1^f,\ldots,\psi_{nens}^f$ are the individual model forecasts, for each of the *nens* ensemble members. Ψ^f is a *nstate*×*nens* matrix where *nstate* is the number of model states. The state error covariance matrix of the model is directly calculated from the spread between the different ensemble members using

$$P^f=\overline{(\Psi^f-\Psi^t)(\Psi^f-\Psi^t)^T} \tag{4}$$

where Ψ^t is the true model state *nstate*×*nens* matrix. Since the true state is not known, it is assumed that

$$P^f \approx P_e^f=\overline{(\Psi^f-\overline{\Psi^f})(\Psi^f-\overline{\Psi^f})^T} \tag{5}$$

where $\overline{\Psi^f}$ represents the ensemble average and it is assumed that the ensemble of model predictions is unbiased. The observations matrix, Y, is a *nobs*×*nens* matrix containing the observations, where *nobs* is the number of observations. Y is given by

$$Y=H\Psi^t+\epsilon \tag{6}$$

where H is a *nobs*×*nstate* transforming Ψ^t to the observations and ϵ the random error in the observations. ϵ is random noise with a zero mean and an standard deviation given by R, the measurement error covariance (*nobs*×*nobs* matrix). In this study, H ensures a spatial match between the satellite observations and modeled soil moisture from the model. This leads to the general form of the EnKF:

$$\begin{aligned}\Psi^a=\Psi^f+P^fH^T(HP^fH^T+R)^{-1}\\ \times(Y-H\Psi^f)\end{aligned} \tag{7}$$

Apart from state-augmentation, the EnKF also allows model parameters of the LISFLOOD model to be estimated in the same update moment. Since there are no observations of the parameters, matrix Y remains the same. However, the matrix Ψ^f and measurement operator are extended with 14 rows to enable the

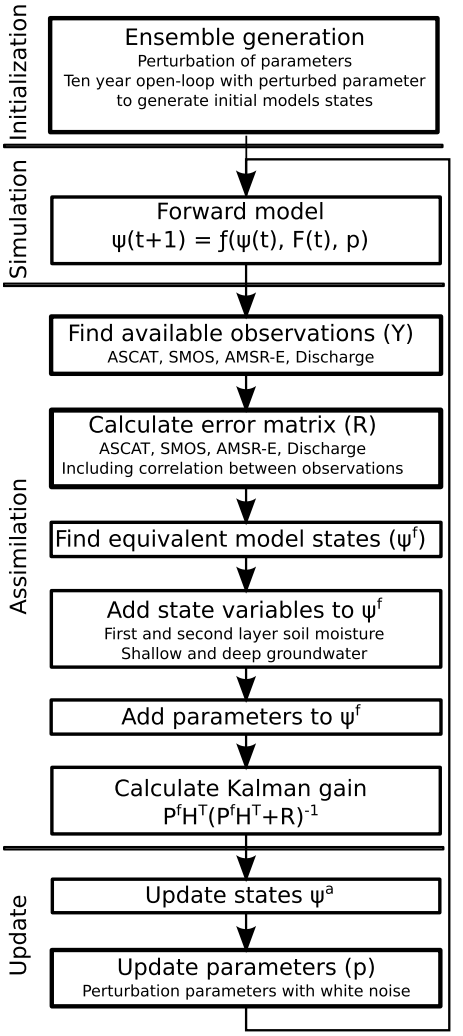

Figure 3. Flowchart of data assimilation scheme.

parameters of Table 1 to be estimated at the update moment. This results in updated parameters in Ψ^a which are perturbed by multiplication white noise with a standard deviation of 0.01, to prevent ensemble deterioration. The perturbations are given by

$$Ln(p'_t) = Ln(p) + W(0, 0.01) \quad (8)$$

where p'_t are the perturbed parameters and $W(0,0.01)$ is white noise with a mean of 0 and standard deviation of 0.01 (–). These new parameters are then used to propagate the model to the next update moment using equation (2).

A relaxation factor β of 0.7 is used for the parameter updating, to prevent strong updates of Ψ^a as a result of erroneous measurements which could result in nonfeasible updates of parameters. Additionally, a β of 0.7 ensures that observations at the end of the calibration still can impact the parameter calibration. If no relaxation factor is applied, the estimated uncertainty of the model predictions (P^f) is small compared to R and no updates would occur anymore at the end of the calibration period. This is particularly important because some observations get more abundant over time due to an improvement in the algorithms of the remotely sensed soil moisture. Especially in a scenario where multiple observations are used (e.g., discharge and multiple satellites), this will ensure that all observations contribute to the calibration. A β of 0.7 was selected as the best value, to ensure convergence of the parameters and allows all sensor to be used in the parameter estimation. The introduction of β results in a modified form of equation (7) for parameter updating:

$$\Psi_p^a = \beta\Psi_p^f + (1-\beta)P^f H^T (HP^f H^T + R)^{-1}(Y - H\Psi_p^f) \quad (9)$$

where Ψ_p^a and Ψ_p^f are the parameter analysis and parameter forecast, respectively. This theoretical framework has been successfully applied in other studies to estimate both state and parameters [e.g., *Tong et al.*, 2012].

Due to small sample sizes and a small number of observations, spurious correlations could occur. This would result in update of parameters that have no physical relation with the observations. To avoid the effects of these unwanted updates of parameters, the covariance between the observations and these parameters is set to zero. This is done for the parameters at the bottom half of Table 1. Given the relations defined in the model structure, it is not possible that the satellite observations contain information on the values of these parameters.

The soil moisture and discharge observations are used to correct the states in the model using equation (7). The soil moisture observations are directly used in the data assimilation system to correct the soil moisture content of the different layers. The error covariance between the different soil layers is calculated from equation (5). Discharge observations are used to correct the groundwater states. Since the discharge observations are strongly related to the groundwater, they contain a large amount of information on the groundwater storage and can be used to correct the groundwater simulations. Other advantages of the correction of the groundwater is that the update will have a larger impact on discharge simulations for the next time step, while updating the river water levels will only result in an improvement in the discharge simulation for a short period (up to 6 days maximum for the Upper Danube).

For the assimilation of the satellite data with the Ensemble Kalman Filter (EnKF), spatial information on the measurements error covariance (R, equation (7)) is required. The structure of R is determined using the data of *Wanders et al*. [2012] over Spain as obtained using high resolution modeling of the unsaturated zone. From this study, the relative errors of each satellite product were determined as well as the spatial correlation of the errors of the satellites. Because *Wanders et al*. [2012] did not include the spatial correlation between the satellite errors of different sensors, the cross-variograms between sensors were additionally calculated using the same data set (Appendix A). The error covariance between the discharge observations is set to zero while the error for the discharge observations is assumed to be 30% of the discharge [e.g., *Di Baldassarre and Montanari*, 2009]. It is also assumed that there is no error covariance between the satellite observations and discharge observations.

2.5. Scenarios

To test if the Ensemble Kalman Filter calibration framework is capable to calibrate known parameters and reproduce these results with different prior distributions, a synthetic data set was used for a calibration experiment. Using known parameters, a synthetic data set was produced and used as synthetic observations for parameter estimation and state updates. Both discharge and synthetic satellite observations are reproduced with the synthetic experiment. The framework was tested with the assimilation of one synthetic discharge observation in combination with multisensor synthetic soil moisture observations for a period of 2 year. The errors assumed for the synthetic observations are identical to those of the real observations. For the synthetic discharge, a 30% error and an error of 0.05 $m^3\ m^{-3}$ for all of the synthetic ASCAT, AMSR, and SMOS observations are assumed. ASCAT and AMSR-E synthetic observations are created from the 0–2 cm soil moisture layer, while SMOS synthetic observations are generated from the average of the two first soil moisture layers (0–5 cm). A total of 300 ensemble members is used for the synthetic experiment, which is identical to the number used for the calibration of other scenarios. It was tested whether calibrated parameters are found to be identical to the parameter set used to create the synthetic data set.

After the synthetic experiment, a sensitivity analysis was performed on the LISFLOOD model to enable better interpretation of the results. This sensitivity experiment is complementary to the normal sensitivity analysis of LISFLOOD, which is described by *Van Der Knijff et al*. [2010]. Since the LISFLOOD was modified for the assimilation of remotely sensed soil moisture, this new sensitivity analysis is required. All parameters (Table 1) were modified by taking the 90% and 110% of the prior mean. The discharge and soil moisture dynamics as well as the absolute levels of these variables have been related to all calibration parameters of the model. The variance is computed for each of these variables to estimate the dynamic behavior, while the absolute levels are computed by taking the long-term mean.

After these initial experiments, observations of three microwave satellites and seven discharge time series were used to estimate the parameters of the LISFLOOD model for the Upper Danube area using the Ensemble Kalman Filter. Different calibration scenarios were tested, each using different observations or combinations of observations. This is done to obtain understanding of the influence of the observations on the retrieved parameters and their capacity to estimate the parameters. A detailed description of the calibrated parameters, updated state variables, total number of observations, and the total number of scenarios can be found in Table 3. The calibration scenarios included are as follows:

1. One satellite soil moisture product, ASCAT, AMSR-E, or SMOS.
2. Discharge observations, either one or seven locations (Figure 1).
3. Discharge observations (one or seven locations) and one satellite soil moisture product.
4. Discharge observations (one or seven locations) and all satellite products.

The individual scenarios were calibrated for a 2 year period (2010–2011). This period was chosen because of the availability of all three microwave soil moisture satellite products. When all three satellite products are used, ASCAT and AMSR-E are directly compared to 0–2 cm simulated soil moisture and SMOS is compared to the weighted average of the two first simulated soil moisture layers (0–2 and 2–5 cm). The updates of the two soil moisture layers are dependent on the specific uncertainty of the satellite observation and the uncertainty in the modeled soil moisture. The satellite observations are directly compared to the simulated soil moisture at their specific penetration depth to reduce errors in the assimilation.

Table 3. Detailed Description of the Calibration Scenarios[a]

	Number of Observations			
Scenario	Soil Moisture	Discharge	Calibrated Parameters	Updated State Variables
No assimilation	0	0	None	None
ASCAT	81,000	0	Soil	Topsoil
AMSR-E	223,000	0	Soil	Topsoil
SMOS	92,000	0	Soil	Topsoil
All satellites	396,000	0	Soil	Topsoil
1 discharge station	0	730	All	Topsoil & GW
7 discharge stations	0	5000	All	Topsoil & GW
ASCAT + 1 discharge station	81,000	730	All	Topsoil & GW
AMSR-E + 1 discharge station	223,000	730	All	Topsoil & GW
SMOS + 1 discharge station	92,000	730	All	Topsoil & GW
All satellites + 1 discharge station	396,000	730	All	Topsoil & GW
ASCAT + 7 discharge stations	81,000	5000	All	Topsoil & GW
AMSR-E + 7 discharge stations	223,000	5000	All	Topsoil & GW
SMOS + 7 discharge stations	92,000	5000	All	Topsoil & GW
All satellites + 7 discharge stations	396,000	5000	All	Topsoil & GW

[a]Scenario names indicate the assimilated data, the number of observations are divided between remotely sensed soil moisture observations. Calibrated parameters are either soil parameters (Soil), including *SnCoef*, $KSat_1$, $KSat_2$, c_{pref}, and b_{xin}. Finally, the updated state variables are given, where Topsoil indicates the first two layers of the LISFLOOD model and GW both groundwater reservoirs of the LISFLOOD model.

The calibrated parameters found at the end of the calibration period for the different scenarios were used to simulate discharge for the period 2000–2009 as a validation of the model. All 300 members from the ensemble found by calibration were used in the validation to determine the uncertainty in the simulated discharge and soil moisture. No assimilation of observations was performed during the validation, to only validate the performance of the calibrated model without data assimilation. From this ensemble, the ensemble mean discharge and soil moisture were calculated and compared with the observed discharge and soil moisture. The performance of the soil moisture simulations was evaluated with time series of AMSR-E (2002–2009) and ASCAT (2007–2009). These time periods were selected because these data are not used during the calibration of the LISFLOOD model and are therefore considered to be independent, although it is acknowledged that independent observations would have been better. The performance of the calibration scenarios was also compared with a simulation using the prior distributions of parameters (baseline scenario).

In the validation, the root-mean-square error of the discharge and soil moisture simulations was calculated by

$$RMSE = \sqrt{\frac{\sum_{t=1}^{T} (Z_{mod}(t) - Z_{obs}(t))^2}{T}} \tag{10}$$

where Z_{mod} is the modeled ensemble mean discharge or soil moisture, Z_{obs} is the observed discharge or soil moisture, and T is the total number of observations, approximately 3600 for discharge and between 81,000 and 396,000 for the satellite observations (dependent on the scenario). To enable comparison between discharge time series of different stations, the *RMSE* of a station is standardized on the average discharge of the station ($\overline{Q_{obs}}$) using

$$SRMSE = \frac{RMSE}{\overline{Q_{obs}}} \tag{11}$$

where *SRMSE* is the normalized root-mean-square error of the discharge location and $\overline{Q_{obs}}$ is the average observed discharge ($m^3\ s^{-1}$).

3. Results

3.1. Calibration on Synthetic Data Set and Sensitivity Analysis

The synthetic calibration experiment was repeated 6 times using 300 ensemble members and different realizations of the prior distribution showing consistent results for every repetition. Parameters used to produce

the synthetic data set were within the 95% confidence interval of the calibrated parameter distributions (Figure 4), with the exception of GW_{perc}. This is caused by the low sensitivity of the model to changes in this parameter compared to changes in T_{lz}. The synthetic discharge could be reproduced with a *SRMSE* of 0.06 at the outlet of the Upper Danube. From these results, it is concluded that the EnKF calibration framework shows a consistent performance and could be used with confidence to calibrate scenarios based on satellite and discharge observations. The framework can be used with confidence to calibrate large-scale hydrological models and distributed land-surface models in general.

The results of the sensitivity analysis are presented in Table 4 and show that the soil moisture is very sensitive to, in decreasing order of importance, c_{pref}, b_{xin}, $KSat_1$, *SnCoef*, and $KSat_2$. The parameters in the bottom half of Table 1 do not have any impact on the soil moisture simulation and hence it is justified to assume no correlation between these parameters and soil moisture observations during the data assimilation.

The discharge dynamics and total discharge volumes are sensitive to changes in all parameters (Table 1). The largest sensitivity of the total runoff is to $KSat_1$, b_{xin}, T_{lz}, c_{pref}, GW_{prec}, and *SnCoef* (in decreasing order of importance). Part of the impact of the parameters related to overland flow is caused by the contribution of surface runoff to the total discharge. Additionally, the evapotranspiration rate largely determines the total discharge volume of the catchment. Evapotranspiration is controlled by the infiltration rate of soil moisture through the unsaturated zone and hence is strongly related to b_{xin} and $KSat_1$. Discharge dynamics are sensitive to c_{pref}, b_{xin}, GW_{perc}, T_{uz}, *CalMan*, $KSat_1$, $Chan_{N2}$, and $KSat_2$.

3.2. Parameter Identification

The calibrated parameters for all calibration scenarios show that including more discharge and soil moisture observations leads to decreased spread in the calibrated parameters (Figure 5). Including multiple discharge observation time series instead of one leads to a better identification of parameters (Figure 5) as is expected from the increased amount of information given to the calibration framework.

When both discharge and soil moisture observations are used for the parameter estimation and state updates of the LISFLOOD model, parameters related to land-surface processes, e.g., saturated hydraulic conductivity, are better identified, resulting in posterior parameter distributions with a low uncertainty (Figure 5). The uncertainty of surface parameters calibrated with only discharge observations is significantly higher compared to the calibration with both soil moisture and discharge observations. This confirms that discharge observations contain less information on processes related to the unsaturated zone than soil moisture observations and are more informative regarding processes in the groundwater system and channel routing. Satellite observations will contribute to the calibration and contain information on land-surface processes that cannot be inferred from discharge observations. When soil moisture observations are added to the calibration, some small changes can be found in the groundwater parameters. This is related to the fact that some parameters impact both discharge and soil moisture simulations (e.g., $KSat_1$ and b_{xin}). When these parameters are modified, also other parameters impacting discharge should be modified to compensate for changes in the input from the soil moisture, to correctly simulate the discharge in the catchment.

The uncertainty found in calibrated parameters by calibration with ASCAT is lower than with AMSR-E or SMOS soil moisture (not shown), which could be caused by the smaller error in the ASCAT soil moisture product used in the data assimilation system [*Wanders et al.*, 2012] or higher spatial resolution of the ASCAT product. For this study, it was assumed that the error structure of *Wanders et al.* [2012] is identical to the error structure of the microwave remote sensing observations for the Upper Danube, which could also impact the results. Additionally, the number of observations used for the calibration with ASCAT is also significantly higher than for calibration with either AMSR-E or SMOS (Table 3). This result is not dependent on the addition of discharge observations. More research is required to see if this result is also valid for other areas and independent of model structure and calibration framework.

3.3. Discharge Simulation

Time series for the validation of the discharge at the outlet of the Upper Danube show that without the EnKF data assimilation, the discharge is on average underestimated for both peak flows and base flow (Figure 6). In all calibration scenarios, the estimation of discharge is improved compared to the no calibration scenario; especially the base flow has increased to levels more similar to those observed during low flow periods. Depending on the different satellites used for the calibration, the *SRMSE* is decreased

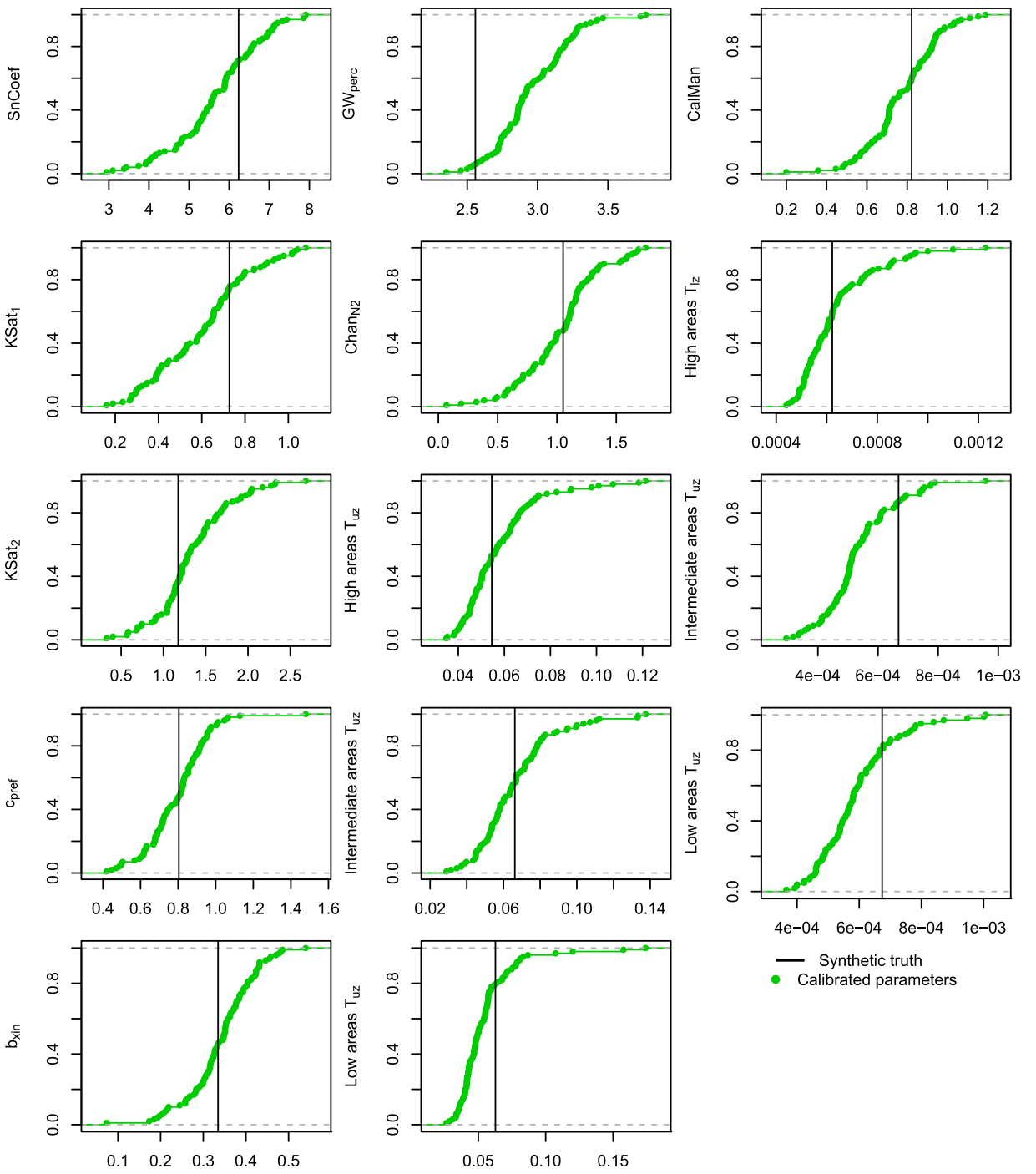

Figure 4. The calibrated parameter distributions for the synthetic experiment used in the simulation of discharge in the LISFLOOD model. In black, the parameter set used to create the synthetic data set is shown, green indicates the calibrated parameter set based on the synthetic data. With the exception of GW_{perc}, all parameters are within the 95% confidence interval of their true values used to generate the synthetic data. Description of the parameters is given in Table 1.

by ≈ 10% compared to no calibration (Figures 7 and 8). The improvement in discharge simulation is the largest for AMSR-E and lower for ASCAT and SMOS. Although parameter uncertainties are smaller for ASCAT, calibration did not necessarily lead to better discharge simulations. For SMOS, the performance could be hampered by the relatively large number of missing data (masked). This is due to Radio Frequency Interference (RFI), which has a big impact on the data quality of SMOS in this region [*Dall'Amico et al.,* 2012]. The error of SMOS satellite retrievals used in this study is also relatively large compared to

Table 4. The Dependency of Mean Soil Moisture (Θ), Variance in Soil Moisture ($var(\Theta)$), Mean Discharge (Q), and the Variance in Discharge ($var(Q)$) to Changes in Individual Parameters ($\Delta\alpha$)

	$\frac{\Delta\Theta}{\Delta\alpha}$	$\frac{var(\Theta)}{\Delta\alpha}$	$\frac{\Delta Q}{\Delta\alpha}$	$\frac{\Delta var(Q)}{\Delta\alpha}$
SnCoef	265	0.040	2638	−0.0005
$KSat_1$	−415	0.142	−14,068	−0.03
$KSat_2$	3	0.001	1.21	0.002
c_{pref}	1835	−0.087	−8891	0.103
b_{xin}	1600	−0.163	13,419	0.090
T_{uz}	0.0	0.0	484	0.064
T_{lz}	0.0	0.0	9115	0.001
GW_{perc}	0.0	0.0	−2649	0.069
$Chan_{N2}$	0.0	0.0	−6	−0.008
CalMan	0.0	0.0	−11	0.032

the other two satellites, which in combination with a reduced number of observations leads to a decreased performance in the calibration.

For the simulation of discharge at the catchment outlet, the calibration on only one station shows a lower *SRMSE* (equation (11)) compared to calibration on more discharge observations, or calibration on both discharge and satellite observations (Figure 7). This is caused by the fact that the discharge location used for calibration on only one station is situated close to the catchment outlet (large square in Figure 1). Therefore, calibration parameters are only adjusted to give the best simulation of the discharge at the outlet as possible, while other calibration scenarios also aim at satisfying other calibration criteria. The average *SRMSE* for all validation locations (Figure 1) is reduced when the LISFLOOD model is calibrated using seven discharge observations compared to only calibration on one discharge observation (Figure 8). This decrease is found for all scenarios that include seven discharge locations, with or without the addition of satellite observations. This leads to the conclusion that increasing the number of discharge locations will not necessarily increase the accuracy of discharge simulations at the outlet. However, it will result in a better simulation of the distribution of runoff and thereby improve overall discharge simulation throughout the catchment. Overall, the discharge simulation for the validation period is improved by $\approx$ 15% compared to calibration only on discharge at the outlet, as shown by a decrease in the *SRMSE* (Figure 8).

Throughout the catchment, the calibration with remote sensed soil moisture improved discharge simulation in the upstream part of the catchment (*t* test 95% confidence). However, no catchment above 40,000 km^2 showed any significantly improved discharge simulation as a result of calibration on one or multiple sources of remotely sensed soil moisture. Calibrations with seven discharge locations and ASCAT, AMSR-E, SMOS, or a combination of satellites are compared to a scenario with only calibration on seven discharge locations (Figure 9). Only locations where the discharge is decreased or increased by more than 5% are shown. From this spatial comparison, it is concluded that discharge simulations are improved in the upstream areas when soil moisture is added to the calibration.

Compared to calibration with only discharge, calibration with discharge and satellite data does improve discharge simulations for smaller catchments. From these results, it is concluded that adding satellite data to the calibration will mostly improve the overall discharge results in situations when no discharge data are available for calibration. In these situations, satellite observations lead to small improvements of discharge simulations.

3.4. Soil Moisture Simulation

Soil moisture simulation of the LISFLOOD model after calibration on discharge or satellite observations is compared with time series of AMSR-E (2002–2009) and ASCAT (2007–2009). After calibration, an improvement is found compared to the soil moisture simulation with the prior distribution. Compared to observed AMSR-E and ASCAT data, the average *RMSE* is reduced from 0.24 (prior distribution) to 0.058 $m^3\ m^{-3}$ after calibration on multisensor satellite observations. However, no difference could be found between the different scenarios, using one or multiple satellite products. When the scenarios are compared spatially some distinct patterns are found. The improvements for calibration with ASCAT and AMSR-E are mainly found in the mountainous areas as can be seen in Figure 9. This could be related to the relatively poor model simulation of the unsaturated zone in these regions in the scenario without calibration, leading to a large improvement. Additionally, in these regions the observation error of ASCAT and AMSR-E is lower than for SMOS [*Wanders et al.*, 2012]. The combination of these two factors leads to large improvements in mountainous areas, which would normally not be expected because of the low quality of remotely sensed soil moisture retrievals in these areas. Calibration on SMOS data only improves soil moisture in the lowland regions, which could be related to the increased observation depth of the SMOS satellite compared to the other sensors. If all satellite data are used at the same time to calibrate the LISFLOOD model, simulated soil

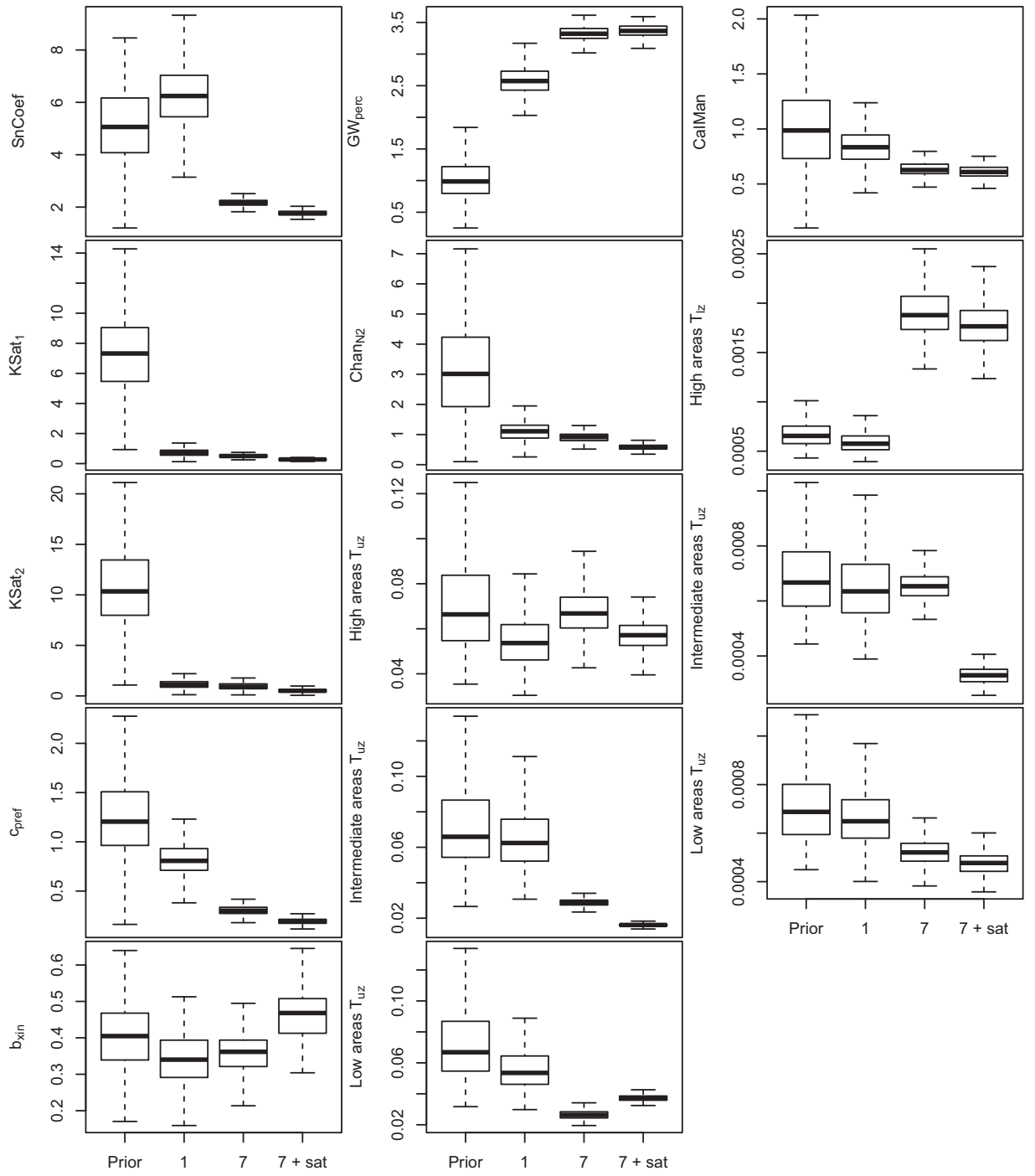

Figure 5. The calibrated parameter distributions for three different calibration scenarios and the prior parameter estimations used in the simulation of discharge in the LISFLOOD model. Prior is based on expert knowledge and used as prior for the other scenarios, 1 is calibration on one discharge station close to the outlet (Figure 1), 7 is calibration based on seven stations distributed across the catchment, and 7 + sat is calibration based on seven discharge stations and remotely sensed soil moisture by three microwave satellite sensors (SMOS, AMSR-E, and ASCAT). Description of the parameters is given in Table 1.

moisture patterns are improved for large parts of the catchment, without favoring specific regions. This is caused by the fact that single satellite improvements are compensated by other sensors and a more widespread improvement is the result.

As all parameters are spatially lumped (with exception of T_{uz} and T_{lz}), calibration will result in improvements for some areas while the simulation deteriorates for other regions of the Upper Danube. Due to the large

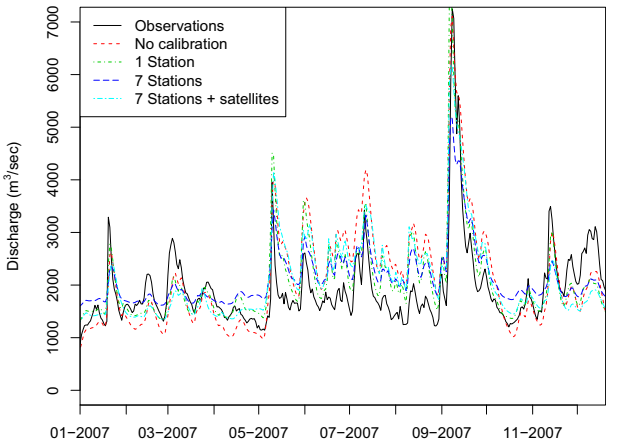

Figure 6. Time series of ensemble mean discharge at the outlet of the Upper Danube catchment, for multiple calibration scenarios: observed indicates the observed discharge time series. Calibration scenarios are as follows: no calibration, a simulation using the prior distribution of parameters based on expert knowledge, 1 station is calibration on one discharge station (Figure 1), 7 stations is calibration based on seven stations, and 7 station + satellites is calibration based on seven discharge stations and remotely sensed soil moisture by three microwave satellite sensors (SMOS, AMSR-E, and ASCAT).

number of parameters, it is not feasible to include a calibration of spatially distributed parameters with the given number of ensemble members, i.e., this would lead to numerical problems for the calibration framework and unidentifiable model parameterizations.

4. Discussion and Conclusion

The LISFLOOD hydrological model was calibrated for the Upper Danube catchment using discharge observations and remotely sensed soil moisture from three different spaceborne sensors. An Ensemble Kalman Filter with augmented state was used to estimate parameters of the LISFLOOD model for a period of 2 years (2010–2011). In total, 10 model parameters were calibrated and used for a validation over a period of 10 years (2000–2009).

The Ensemble Kalman Filter was successfully used to calibrate the model on a synthetic data set with known parameters and state variables. All parameters could be successfully identified using synthetic observations of discharge and satellite soil moisture. It is concluded that the Ensemble Kalman Filter can be used with confidence to calibrate spatially distributed hydrological models and estimate both state variables and parameters.

Parameters of the LISFLOOD model were identified with reduced uncertainty when soil moisture data were assimilated into the hydrological model. Especially parameters related to land-surface processes showed a strong decrease in parameter uncertainty compared to calibration without soil moisture data. Parameters related to groundwater and routing were better calibrated using one or multiple discharge observations. When more discharge observations were introduced to the calibration framework, uncertainties in parameters, uncertainties in groundwater and routing parameters were reduced.

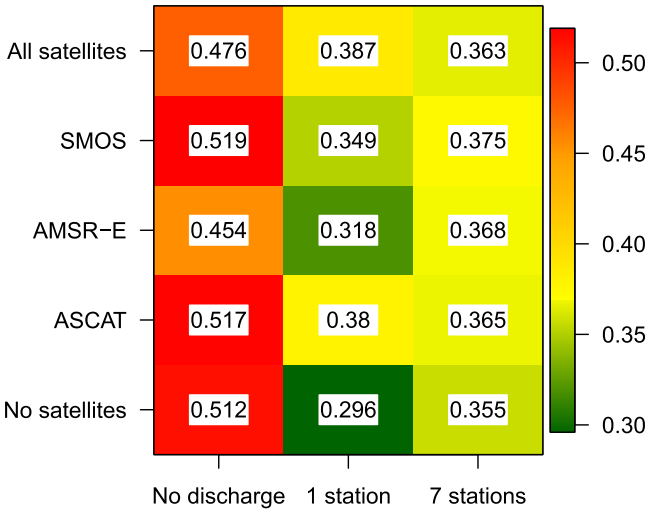

Figure 7. Cross table with the normalized root-mean-square error of the ensemble mean discharge at the outlet of the Upper Danube catchment using 15 different calibration scenarios. Columns indicate calibration without using discharge, 1 discharge location close to the outlet, or 7 discharge locations distributed throughout the catchment. Rows indicate calibration on soil moisture, without using any data or using either data from the ASCAT, AMSR-E, or SMOS satellite or a combination of all three sensors (All satellites).

The use of remotely sensed soil moisture significantly improved the model performance compared to parameters estimated with expert knowledge. However, the results of this study show that the contribution of remotely sensed soil moisture to the improvement of discharge is limited for large catchments. No catchment above 40,000 km^2 showed any

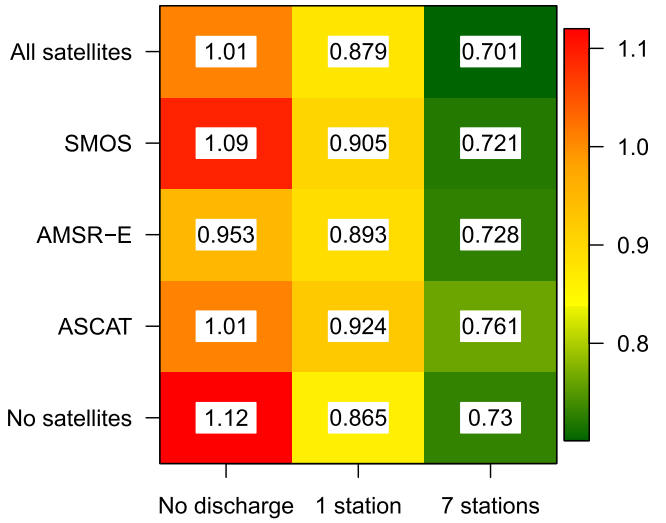

Figure 8. Cross table with the average normalized root-mean-square error of the ensemble mean discharge at all validation locations of the Upper Danube catchment (Figure 1) using 15 different calibration scenarios. Columns indicate calibration without using discharge, 1 discharge location close to the outlet, or 7 discharge locations distributed throughout the catchment. Rows indicate calibration on soil moisture, without using any data or using either data from the ASCAT, AMSR-E, or SMOS satellite or a combination of all three sensors (All satellites).

improved discharge simulations as a result of calibration on one or multiple sources of remotely sensed soil moisture.

On average, small improvements in soil moisture simulations were found for all scenarios that included soil moisture assimilation. Soil moisture simulations are mostly improved for ASCAT and AMSR-E in areas with large relief, where the relative importance of fast runoff processes is larger compared to the topographically flat areas. SMOS showed a different pattern, with improvements in soil moisture simulation mainly observed in flat areas, and SMOS showed relatively smaller improvements in soil moisture simulations. When all three sensors were combined, locally improvements were more averaged out, while on average, simulations of soil moisture throughout the catchment were improved. Compared to soil moisture simulation with the prior distribution

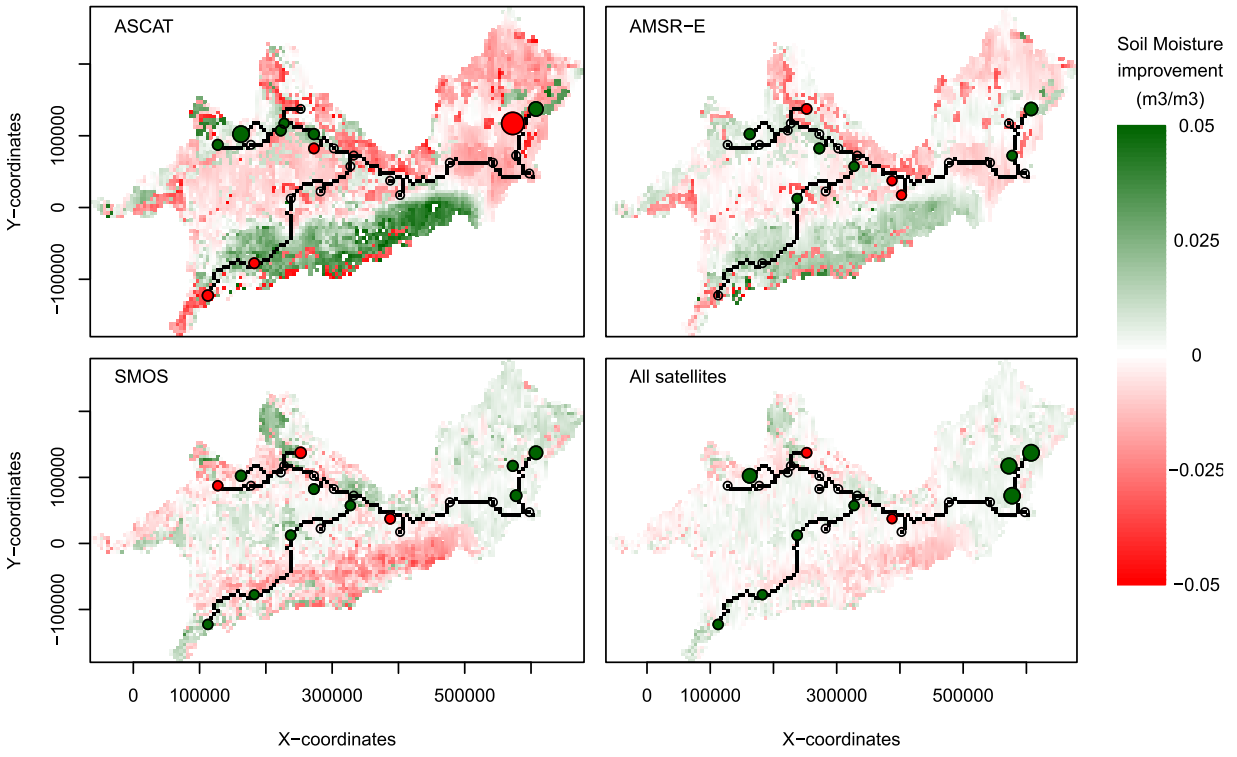

Figure 9. Comparison between calibration on seven discharge locations and calibration based on these discharge locations and remotely sensed soil moisture. Colors indicate the improvement in the soil moisture simulations for the validation period, circles indicate whether any improvement is found for the ensemble mean discharge simulation, size of the circle indicates the relative improvement in the discharge simulations, and blank circles are locations with a less than 5% change compared to the calibration on seven discharge locations. ASCAT is a comparison between the calibration on only discharge and discharge combined with remotely sensed soil moisture observations from ASCAT (similar for AMSR-E and SMOS). All satellites show a comparison between the calibration on only discharge and discharge combined with all three remotely sensed soil moisture observations.

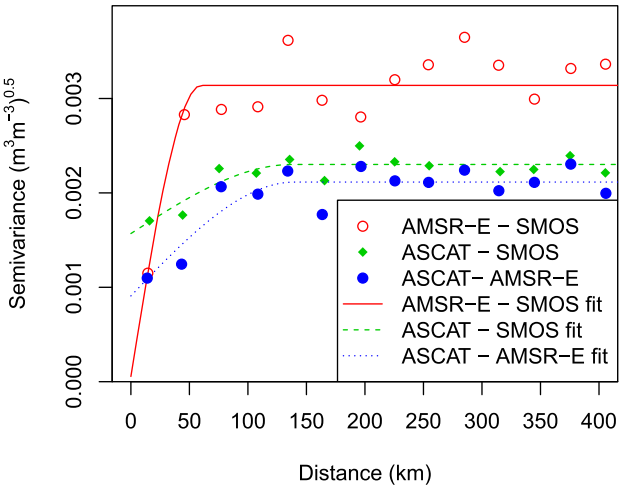

Figure A1. Cross-variograms of the bin-average time-dependent satellite product error calculated for three satellite soil moisture products and a unsaturated zone model, for the period January 2010 to June 2011 over Spain [*Wanders et al*., 2012].

of parameters, all calibration scenarios with remotely sensed soil moisture significantly improved soil moisture simulations.

Compared to calibration with only discharge, calibration with addition of satellite data does improve discharge simulations for smaller catchments. In contrast to *Lee et al*. [2011], in this study only an improvement was found for discharge simulations in small-sized catchments. This small improvement in upstream discharge is also in line with work of *Brocca et al*. [2010]. However, *Brocca et al*. [2010] and *Lee et al*. [2011] both used assimilation of soil moisture during the validation period, which could lead to different results. *Sutanudjaja et al*. [2014] calibrated a hydrological model on soil moisture observations and also found minor improvements in discharge simulations for a large catchment.

It is concluded that remotely sensed soil moisture improves the calibration of the LISFLOOD hydrological model for small catchments, while for larger catchments, above 40,000 km^2, this increase in model performance is negligible due to the large relative importance of groundwater and channel routing.

Increasing the number of discharge observations will improve catchment average discharge simulations, which confirms previous work by *Rakovec et al*. [2012]. Moreover, the error in the discharge simulation at the outlet will not decrease by adding more discharge observations, which is mainly caused by the fact that it is easier to fit a single discharge time series than discharge series at multiple locations simultaneously. This finding is contradictory to *Rakovec et al*. [2012], which might be the result of a larger catchment size in this study. This larger catchment will result in significantly longer travel times of the water, interference of man-made structure, and additionally, a larger grid resolution of the hydrological model. All these factors could cause the difference between this study and work of *Rakovec et al*. [2012].

The addition of soil moisture in the calibration further improves discharge simulations in the upstream areas of the Upper Danube. Additionally, the soil moisture simulation is improved for large parts of the catchment. This leads to the conclusion that a more realistic portrayal of the catchment's hydrology (i.e., being right for the right reason) will thus be achieved by using multiple discharge time series and remotely sensed soil moisture in model calibration.

A point of attention is the availability of discharge and precipitation data for this catchment. The precipitation network in this catchment is very dense, leading to low uncertainties in interpolated precipitation for the Upper Danube. As suggested by *Crow et al*. [2009], remotely sensed soil moisture could be used to correct for uncertainties in precipitation or other meteorological forcing data. Thus, the assimilation of remotely sensed soil moisture for parameter estimation in more sparsely gauged regions could potentially result in larger improvements in discharge and soil moisture simulations than observed in this study.

Appendix A: Cross-Variograms of Errors in Remotely Sensed Soil Moisture Products

To calculate the spatial correlation between the satellite errors of different sensors, cross-variograms of the errors have been calculated using the data from *Wanders et al*. [2012]. The semivariance of the measurements is calculated by computing the distance between two individual observations. The fitted cross-variogram is used to derive the semivariance for these observations. This procedure is repeated for all possible combinations of the satellite observations. Cross-variograms of the error show that the error for the different satellite products is correlated up to a maximum distance of 150 km (Figure A1).

Acknowledgments
This research was funded by a grant from the user support program Space Research of NWO (contract NWO GO-AO/30). EC-JRC is acknowledged for being able to work with the Danube model setup. Due to restrictions of the data license, observed meteorological forcing and discharge time series are not available from the authors. However, the authors can provide the reader with the contact details of the data owners, to obtain the data. The LISFLOOD model and PCRaster data assimilation framework are publicly available and model results of this research are available upon request from the authors. Three anonymous reviewers are acknowledged for their contribution and help to improve the manuscript.

References

Aubert, D., C. Loumagne, and L. Oudin (2003), Sequential assimilation of soil moisture and streamflow data in a conceptual rainfall-runoff model, *J. Hydrol.*, *280*(14), 145–161, doi:10.1016/S0022-1694(03)00229-4.

Bartholmes, J. C., J. Thielen, M. H. Ramos, and S. Gentilini (2009), The European flood alert system EFAS—Part 2: Statistical skill assessment of probabilistic and deterministic operational forecasts, *Hydrol. Earth Syst. Sci.*, *13*(2), 141–153, doi:10.5194/hess-13-141-2009.

Bisselink, B., E. van Meijgaard, A. J. Dolman, and R. A. M. De Jeu (2011), Initializing a regional climate model with satellite-derived soil moisture, *J. Geophys. Res.*, *116*, D02121, doi:10.1029/2010JD014534.

Bolten, J., W. Crow, X. Zhan, T. Jackson, and C. Reynolds (2010), Evaluating the utility of remotely sensed soil moisture retrievals for operational agricultural drought monitoring, *IEEE J. Selec. Top. Appl. Earth Obs. Remote Sens.*, *3*(1), 57–66, doi:10.1109/JSTARS.2009.2037163.

Brocca, L., F. Melone, T. Moramarco, W. Wagner, V. Naeimi, Z. Bartalis, and S. Hasenauer (2010), Improving runoff prediction through the assimilation of the ASCAT soil moisture product, *Hydrol. Earth Syst. Sci.*, *14*(10), 1881–1893, doi:10.5194/hess-14-1881-2010.

Brocca, L., T. Moramarco, F. Melone, W. Wagner, S. Hasenauer, and S. Hahn (2012), Assimilation of surface- and root-zone ASCAT soil moisture products into rainfall runoff modeling, *IEEE Trans. Geosci. Remote Sens.*, *50*(7), 2542–2555, doi:10.1109/TGRS.2011.2177468.

Burgers, G., P. Van Leeuwen, and G. Evensen (1998), Analysis scheme in the Ensemble Kalman Filter, *Mon. Weather Rev.*, *126*, 1719–1724.

Camporese, M., C. Paniconi, M. Putti, and P. Salandin (2009), Ensemble Kalman Filter data assimilation for a process-based catchment scale model of surface and subsurface flow, *Water Resour. Res.*, *45*, W10421, doi:10.1029/2008WR007031.

Clark, M. P., D. E. Rupp, R. A. Woods, X. Zheng, R. P. Ibbitt, A. G. Slater, J. Schmidt, and M. J. Uddstrom (2008), Hydrological data assimilation with the Ensemble Kalman Filter: Use of streamflow observations to update states in a distributed hydrological model, *Adv. Water Resour.*, *31*(10), 1309–1324, doi:10.1016/j.advwatres.2008.06.005.

Crow, W. T., G. J. Huffman, R. Bindlish, and T. J. Jackson (2009), Improving satellite-based rainfall accumulation estimates using spaceborne surface soil moisture retrievals, *J. Hydrometeorol.*, *10*(1), 199–212, doi:10.1175/2008JHM986.1.

Crow, W. T., D. G. Miralles, and M. H. Cosh (2010), A quasi-global evaluation system for satellite-based surface soil moisture retrievals, *IEEE Trans. Geosci. Remote Sens.*, *48*(6), 2516–2527.

Dall'Amico, J., F. Schlenz, A. Loew, and W. Mauser (2012), First results of SMOS soil moisture validation in the upper Danube catchment IEEE Trans, *Geosci. Remote Sens.*, *50*, 1507–1516, doi: 10.1109/TGRS.2011.2171496.

De Jeu, R. A. M., W. Wagner, T. R. H. Holmes, A. J. Dolman, N. C. Van de Giesen, and J. Friesen (2008), Global soil moisture patterns observed by space borne microwave radiometers and scatterometers, *Surv. Geophys.*, *28*, 399–420, doi:10.1007/s10712-008-9044-0.

de Rosnay, P., M. Drusch, D. Vasiljevic, G. Balsamo, C. Albergel, and L. Isaksen (2013), A simplified extended Kalman filter for the global operational soil moisture analysis at ECMWF, *Q. J. R. Meteorol. Soc.*, *139*(674), 1199–1213, doi:10.1002/qj.2023.

Dharssi, I., K. J. Bovis, B. Macpherson, and C. P. Jones (2011), Operational assimilation of ASCAT surface soil wetness at the Met Office, *Hydrol. Earth Syst. Sci.*, *15*(8), 2729–2746, doi:10.5194/hess-15-2729-2011.

Di Baldassarre, G., and A. Montanari (2009), Uncertainty in river discharge observations: A quantitative analysis, *Hydrol. Earth Syst. Sci.*, *13*(6), 913–921, doi:10.5194/hess-13-913-2009.

Dorigo, W. A., K. Scipal, R. M. Parinussa, Y. Y. Liu, W. Wagner, R. A. M. de Jeu, and V. Naeimi (2010), Error characterisation of global active and passive microwave soil moisture datasets, *Hydrol. Earth Syst. Sci.*, *14*(12), 2605–2616, doi:10.5194/hess-14-2605-2010.

Dorigo, W. A., et al. (2011), The international soil moisture network: A data hosting facility for global in situ soil moisture measurements, *Hydrol. Earth Syst. Sci.*, *15*(5), 1675–1698, doi:10.5194/hess-15-1675-2011.

Draper, C., J.-F. Mahfouf, J.-C. Calvet, E. Martin, and W. Wagner (2011), Assimilation of ASCAT near-surface soil moisture into the SIM hydrological model over France, *Hydrol. Earth Syst. Sci.*, *15*(12), 3829–3841, doi:10.5194/hess-15-3829-2011.

Draper, C. S., J. P. Walker, P. J. Steinle, R. A. M. de Jeu, and T. R. H. Holmes (2009), An evaluation of AMSR-E derived soil moisture over Australia, *Remote Sens. Environ.*, *113*, 703–710.

Draper, C. S., R. H. Reichle, G. J. M. De Lannoy, and Q. Liu (2012), Assimilation of passive and active microwave soil moisture retrievals, *Geophys. Res. Lett.*, *39*, L04401, doi:10.1029/2011GL050655.

Evensen, G. (1994), Sequential data assimilation with a nonlinear quasi-geostrophic model using Monte Carlo methods to forecast error statistics, *J. Geophys. Res.*, *99*(C5), 10,143–10,162, doi:10.1029/94JC00572.

Evensen, G. (2003), The Ensemble Kalman Filter: Theoretical formulation and practical implementation, *Ocean Dyn.*, *53*, 343–367, doi: 10.1007/s10236-003-0036-9.

Evensen, G. (2009), The Ensemble Kalman Filter for combined state and parameter estimation, *IEEE Control Syst.*, *29*(3), 83–104, doi: 10.1109/MCS.2009.932223.

Hendricks Franssen, H. J., H. P. Kaiser, U. Kuhlmann, G. Bauser, F. Stauffer, R. Müller, and W. Kinzelbach (2011), Operational real-time modeling with Ensemble Kalman Filter of variably saturated subsurface flow including stream-aquifer interaction and parameter updating, *Water Resour. Res.*, *47*, W02532, doi:10.1029/2010WR009480.

Karssenberg, D., O. Schmitz, P. Salamon, K. de Jong, and M. F. P. Bierkens (2010), A software framework for construction of process-based stochastic spatio-temporal models and data assimilation, *Environ. Modell. Software*, *25*(4), 489–502, doi:10.1016/j.envsoft.2009.10.004.

Kerr, Y., et al. (2012), The SMOS soil moisture retrieval algorithm, *IEEE Trans. Geosci. Remote Sens.*, *50*(5), 1384–1403, doi:10.1109/TGRS.2012.2184548.

Komma, J., G. Blschl, and C. Reszler (2008), Soil moisture updating by Ensemble Kalman Filtering in real-time flood forecasting, *J. Hydrol.*, *357*(34), 228–242, doi:10.1016/j.jhydrol.2008.05.020.

Le Dimet, F.-X., and O. Talagrand (1986), Variational algorithms for analysis and assimilation of meteorological observations: Theoretical aspects, *Tellus, Ser. A*, *38A*(2), 97–110, doi:10.1111/j.1600-0870.1986.tb00459.x.

Lee, H., D.-J. Seo, and V. Koren (2011), Assimilation of streamflow and in situ soil moisture data into operational distributed hydrologic models: Effects of uncertainties in the data and initial model soil moisture states, *Adv. Water Resour.*, *34*(12), 1597–1615.

Liu, Q., R. H. Reichle, R. Bindlish, M. H. Cosh, W. T. Crow, R. de Jeu, G. J. M. De Lannoy, G. J. Huffman, and T. J. Jackson (2011), The contributions of precipitation and soil moisture observations to the skill of soil moisture estimates in a land data assimilation system, *J. Hydrometeorol.*, *12*(5), 750–765, doi:10.1175/JHM-D-10-05000.1.

Loew, A., T. R. H. Holmes, and R. A. M. De Jeu (2009), The European heat wave 2003: Early indicators from multisensoral microwave remote sensing?, *J. Geophys. Res.*, *114*, D05103, doi:10.1029/2008JD010533.

Lü, H., Z. Yu, Y. Zhu, S. Drake, Z. Hao, and E. A. Sudicky (2011), Dual state-parameter estimation of root zone soil moisture by optimal parameter estimation and extended Kalman filter data assimilation, *Adv. Water Resour.*, *34*(3), 395–406, doi:10.1016/j.advwatres.2010.12.005.

McMillan, H. K., E. O. Hreinsson, M. P. Clark, S. K. Singh, C. Zammit, and M. J. Uddstrom (2013), Operational hydrological data assimilation with the recursive Ensemble Kalman Filter, *Hydrol. Earth Syst. Sci.*, *17*(1), 21–38, doi:10.5194/hess-17-21-2013.

Mendoza, P. A., J. McPhee, and X. Vargas (2012), Uncertainty in flood forecasting: A distributed modeling approach in a sparse data catchment, *Water Resour. Res.*, *48*, W09532, doi:10.1029/2011WR011089.

Merz, B., and E. Plate (1997), An analysis of the effects of spatial variability of soil and soil moisture on runoff, *Water Resour. Res.*, *33*(12), 2909–2922, doi:10.1029/97WR02204.

Montzka, C., H. Moradkhani, L. Weihermüller, H.-J. H. Franssen, M. Canty, and H. Vereecken (2011), Hydraulic parameter estimation by remotely-sensed top soil moisture observations with the particle filter, *J. Hydrol.*, *399*(34), 410–421, doi:10.1016/j.jhydrol.2011.01.020.

Naeimi, V., K. Scipal, Z. Bartalis, S. Hasenauer, and W. Wagner (2009), An improved soil moisture retrieval algorithm for ERS and METOP scatterometer observations, *IEEE Trans. Geosci. Remote Sens.*, *47*(7), 1999–2013, doi:10.1109/TGRS.2008.2011617.

Njoku, E., T. J. Jackson, V. Lakshmi, T. Chan, and S. Nghiem (2003), Soil moisture retrieval from AMSR-E, *IEEE Trans. Geosci. Remote Sens.*, *41*(2), 215–229, doi:10.1109/TGRS.2002.808243.

Ntegeka, V., P. Salamon, G. Gomes, H. Sint, V. Lorini, J. Thielen, and H. Zambrano (2013), EFAS-Meteo: A European daily high-resolution gridded meteorological data set for 1990–2011, Technical report EUR 26408, Publ. Off. of the Eur. Union, Luxembourg, doi:10.2788/51262.

Owe, M., R. A. M. De Jeu, and T. R. H. Holmes (2008), Multisensor historical climatology of satellite-derived global land surface moisture, *J. Geophys. Res.*, *113*, F01002, doi:10.1029/2007JF000769.

Pan, M., A. K. Sahoo, and E. F. Wood (2014), Improving soil moisture retrievals from a physically-based radiative transfer model, *Remote Sens. Environ.*, *140*(0), 130–140, doi:10.1016/j.rse.2013.08.020.

Panagos, P., M. Van Liedekerke, A. Jones, and L. Montanarella (2012), European Soil Data Centre: Response to European policy support and public data requirements. *Land Use Policy*, *29*(2), pp. 329–338, doi:10.1016/j.landusepol.2011.07.003.

Pauwels, V. R., R. Hoeben, N. E. Verhoest, and F. P. D. Troch (2001), The importance of the spatial patterns of remotely sensed soil moisture in the improvement of discharge predictions for small-scale basins through data assimilation, *J. Hydrol.*, *251*(12), 88–102, doi:10.1016/S0022-1694(01)00440-1.

Pauwels, V. R. N., and G. J. M. De Lannoy (2009), Ensemble-based assimilation of discharge into rainfall-runoff models: A comparison of approaches to mapping observational information to state space, *Water Resour. Res.*, *45*, W08428, doi:10.1029/2008WR007590.

Penna, D., H. J. Tromp-van Meerveld, A. Gobbi, M. Borga, and G. Dalla Fontana (2011), The influence of soil moisture on threshold runoff generation processes in an alpine headwater catchment, *Hydrol. Earth Syst. Sci.*, *15*(3), 689–702, doi:10.5194/hess-15-689-2011.

Rakovec, O., A. H. Weerts, P. Hazenberg, P. J. J. F. Torfs, and R. Uijlenhoet (2012), State updating of a distributed hydrological model with Ensemble Kalman Filtering: Effects of updating frequency and observation network density on forecast accuracy, *Hydrol. Earth Syst. Sci.*, *16*(9), 3435–3449, doi:10.5194/hess-16-3435-2012.

Reichle, R. H., D. B. McLaughlin, and D. Entekhabi (2002), Hydrologic data assimilation with the Ensemble Kalman Filter, *Mon. Weather Rev.*, *130*(1), 103–114, doi:10.1175/1520-0493(2002)130<0103:HDAWTE>2.0.CO;2.

Santanello, J., C. D. Peters-Lidard, M. E. Garcia, D. M. Mocko, M. A. Tischler, M. S. Moran, and D. Thoma (2007), Using remotely-sensed estimates of soil moisture to infer soil texture and hydraulic properties across a semi-arid watershed, *Remote Sens. Environ.*, *110*(1), 79–97, doi:10.1016/j.rse.2007.02.007.

Scipal, K., M. Drusch, and W. Wagner (2008), Assimilation of a {ERS} scatterometer derived soil moisture index in the {ECMWF} numerical weather prediction system, *Adv. Water Resour.*, *31*(8), 1101–1112, doi:10.1016/j.advwatres.2008.04.013.

Shepard, D. (1968), A two-dimensional interpolation function for irregularly-spaced data, in *Proceedings of the 1968 23rd ACM National Conference*, ACM '68, pp. 517–524, doi:10.1145/800186.810616.

Sutanudjaja, E. H., S. M. de Jong, F. C. van Geer, and M. F. P. Bierkens (2013), Using ERS spaceborne microwave soil moisture observations to predict groundwater head in space and time, *Remote Sens. Environ.*, *138*, 172–188, doi:10.1016/j.rse.2013.07.022.

Sutanudjaja, E. H., L. P. H. van Beek, S. M. de Jong, F. C. van Geer, and M. F. P. Bierkens (2014), Calibrating a large-extent high-resolution coupled groundwater-land surface model using soil moisture and discharge data, *Water Resour. Res.*, *50*, doi:10.1002/2013WR013807.

Thielen, J., J. Bartholmes, M. Ramos, and A. de Roo (2009), The European flood alert system—Part 1: Concept and development, *Hydrol. Earth Syst. Sci.*, *13*(2), 125–140, doi:10.5194/hess-13-125-2009.

Tong, J.-X., B. X. Hu, and J.-Z. Yang (2012), Using an Ensemble Kalman Filter method to calibrate parameters and update soluble chemical transfer from soil to surface runoff, *Transp. Porous Media*, *91*(1), 133–152, doi:10.1007/s11242-011-9837-3.

Van Der Knijff, J. M., J. Younis, and A. P. J. De Roo (2010), LISFLOOD: A GIS based distributed model for river basin scale water balance and flood simulation, *Int. J. Geogr. Inf. Sci.*, *24*(2), 189–212, doi:10.1080/13658810802549154.

Van Leeuwen, P. J. (2009), Particle filtering in geophysical systems, *Mon. Weather Rev.*, *137*(12), 4089–4114, doi:10.1175/2009MWR2835.1.

Wagner, W., G. Lemoine, and H. Rott (1999), A method for estimating soil moisture from ERS scatterometer and soil data, *Remote Sens. Environ.*, *70*(2), 191–207, doi:10.1016/S0034-4257(99)00036-X.

Wagner, W., G. Blöschl, P. Pampaloni, J. C. Calvet, B. Bizzarri, J. P. Wigneron, and Y. Kerr (2007), Operational readiness of microwave remote sensing of soil moisture for hydrologic applications, *Nord. Hydrol.*, *30*(1), 1–20, doi:10.2166/nh.2007.029.

Wanders, N., D. Karssenberg, M. Bierkens, R. Parinussa, R. de Jeu, J. van Dam, and S. de Jong (2012), Observation uncertainty of satellite soil moisture products determined with physically-based modeling, *Remote Sens. Environ.*, *127*(0), 341–356, doi:10.1016/j.rse.2012.09.004.

Wanders, N., D. Karssenberg, A. de Roo, S. M. de Jong, and M. F. P. Bierkens (2014), The suitability of remotely sensed soil moisture for improving operational flood forecasting, *Hydrol. Earth Syst. Sci.*, *18*(6), 2343–2357, doi:10.5194/hess-18-2343-2014.

Weerts, A. H., and G. Y. H. El Serafy (2006), Particle filtering and Ensemble Kalman Filtering for state updating with hydrological conceptual rainfall-runoff models, *Water Resour. Res.*, *42*, W09403, doi:10.1029/2005WR004093.

Wesseling, C. G., D.-J. Karssenberg, P. A. Burrough, and W. P. A. Van Deursen (1996), Integrating dynamic environmental models in GIS: The development of a dynamic modelling language, *Trans. GIS*, *1*(1), 40–48, doi:10.1111/j.1467-9671.1996.tb00032.x.

Western, A. W., R. B. Grayson, and G. Bloschl (2002), Scaling of soil moisture: A hydrologic perspective, *Annu. Rev. Earth Planet. Sci.*, *30*, 149–180, doi:10.1146/annurev.earth.30.091201.140434.

Erratum

In the originally published version of this article, the second and third initials for coauthor M. F. P. Bierkens were transposed. The citation to Sutanudjaja et al. [2013] on pages 2 and 16 should have been in reference to the following, which should have appeared in the References list: Sutanudjaja, E. H., L. P. H. van Beek, S. M. de Jong, F. C. van Geer, and M. F. P. Bierkens (2014), Calibrating a large- extent high-resolution coupled groundwater-land surface model using soil moisture and discharge data, Water Resour. Res., 50, doi:10.1002/2013WR013807. These errors have since been corrected and this version may be considered the authoritative version of record.